A dynamic analysis of a continuous welded rail track under a longitudinal stress caused by temperature changes

Y Luo[1], **L Li**[1]*, and **H Yin**[2]

[1]Railway and Urban Mass Transit Research Institute, Tongji University, Shanghai, People's Republic of China

[2]Université Paris-Est, UR Navier, Ecole Nationale des Ponts et Chaussées, Champs sur Marme, Marne la Vallée Cedex, Paris, France

The manuscript was received on 23 April 2009 and was accepted after revision for publication on 12 November 2009.

DOI: 10.1243/09544097JRRT290

Abstract: This article presents a dynamic computational model for analysing the correlation between rail's natural frequencies and the longitudinal stress generated by temperature variation. The model includes a rail, sleepers, and the foundation. Some factors such as the rail section profile, rail wear, and the stiffness of fasteners are also considered. Based on the model, numerical computational analyses are performed. The relationship between the rail's longitudinal temperature force and the natural frequency is also studied. The influences of parameters such as the wear of the rail, unsupported distance of adjoining sleepers, fastener stiffness, rail types, and foundation stiffness are investigated. A field experiment is also presented that was performed to investigate the relationship between the rail's dynamic characteristics and the longitudinal stress generated by temperature variation with various unsupported sleeper spacings. The results of analysis and in-field measurements are compared.

Keywords: continuous welded rail track, dynamic characteristics, longitudinal stress, finite-element method

1 INTRODUCTION

At present, a railway track is commonly constructed with the continuous welded rail (CWR). The use of CWR can improve a train's steady operation, reduce the cost of the track, and prolong its service life by removing a large amount of rail joints. However, the use of the CWR track will also introduce a high longitudinal stress caused by temperature changes. For simplicity, the longitudinal stress due to temperature changes is hereafter referred to as the temperature force. The temperature force would lead to the buckling of tracks or the breaking of rails. Trends towards high speeds and heavy-haul railway require a rigorous evaluation of the buckling track's safety. Many experimental and analytical investigations have been carried out to analyse the parameters that may influence the stability of the CWR track and the buckling strength of the CWR, and to predict the CWR's temperature force [**1**–**15**].

The prediction of the temperature force in the CWR track has been studied by various authors for a long time. Various mathematical models have been developed. For instance, the relationship between the rail's transverse vibration and the temperature force of the rail was studied in reference [**11**]. It was concluded that the tension in the rail tends to increase the free vibration frequencies of the rail, whereas the compression tends to reduce the frequencies. Frequency measurement may be a feasible non-destructive method to determine the temperature force.

Luo [**11**] has provided a model for analysing the dynamic characteristics and the trends to alter the CWR track. He also elaborated how the characteristics were affected by the temperature force of the rail. The prediction of this model was compared with field results. It was found that the result of the model differed from that of field measurement. Luo [**11**] simplified the rail on the assumption that the rail was a uniform beam construction with no consideration of the rail section profile, the elastic stiffness, and the

*Corresponding author: Railway and Urban Mass Transit Research Institute, Tongji University, 4800 Cao'an Road, Shanghai 201804, People's Republic of China.
email: lilee@tongji.edu.cn

rotational stiffness of the fasteners. As a result, such a simplification may have some influences on the accuracy of the model. Therefore, it is quite important to build a numerical model to analyse more accurately the dynamic regularities of the CWR track under longitudinal force.

This article presents a dynamic computational model for analysing the correlation between rail natural frequencies and the axial force of the CWR track by means of the finite-element method (FEM). The simulations are performed for different wear levels of the rail and different rail types. At the same time, the sleeper supporting state and the elastic and rotational stiffness of fastener elements are taken into account.

2 A DYNAMIC MODEL OF THE CRW TRACK

2.1 A description of the model

Railway track structure consists of rails, sleepers, a rail pad, and a ballast. Different mathematical simplified models of the railway track system can be developed for different research purposes. The model may include one rail or two parallel rails, and it may be developed in two dimensions or in three dimensions; all these depend on the research objectives [**1**]. This article studies mostly the relationship between the rail's natural frequencies and the longitudinal force caused by varying rail temperatures of the CWR track structure. The model includes only the plane state of vertical vibration of one rail consisting of rails, rail pads, fasteners, sleepers, and ballasts. The model is shown in Fig. 1.

2.2 Rail

The rail model is usually assumed to be a symmetrical beam structure, e.g. an Euler beam or a Timoshenko beam in most cases. Additionally, the rail model can be assumed to be a thin-walled open-section beam structure [**3**]. The influence of all non-linear factors of the track such as the geometric non-linearity of the rail element and the materially non-linear resistance of the ballast can also be considered [**4**]. It has been found that such a simplification in the dynamic analysis of the rail structure will lead to a larger error compared

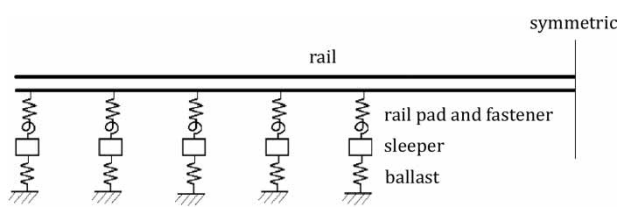

Fig. 1 Model for analysing the dynamic characteristics of the CWR track

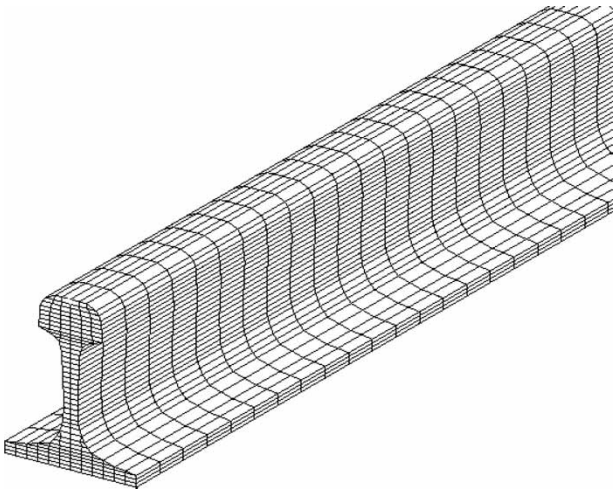

Fig. 2 Mesh elements of a rail

with the track in the field, especially when the dynamic characteristics of the rail itself are analysed.

The main purpose of this article is to study the dynamic characteristics of the rail under a longitudinal force in CWR track structures. To reduce the errors and obtain more accurate results, a finite-element rail model is established to accurately capture the profile of the rail (China standard). A meshed rail is shown in Fig. 2. Rail wear is simulated by changing the rail cross-section shape (shown in Fig. 3). In the dynamic model, the damping of the rail is not taken into account.

The rail elements are solid elements with eight nodes. Their shape functions are

$$N_i = \frac{(1+\xi_i\xi)(1+\eta_i\eta)(1+\zeta_i\zeta)}{8} \tag{1}$$

where ξ_i, η_i, and ζ_i are natural coordinates of node i. According to its geometrical relationship, the calculation formula of the element strain can be described as

$$\varepsilon = \boldsymbol{L}\boldsymbol{u} = \mathbf{B}\boldsymbol{d} = [\mathbf{B}_1\mathbf{B}_2\cdots\mathbf{B}_n]\boldsymbol{d}^e \tag{2}$$

where $\boldsymbol{L}$ is the differential coefficient operator, $\boldsymbol{u}$ is the random displacement vector of the element, $\boldsymbol{d}$ is the displacement vector of a node in the system, and e is the number of elements

$$\mathbf{B}_i = \begin{bmatrix} N_{i,x} & 0 & 0 \\ 0 & N_{i,y} & 0 \\ 0 & 0 & N_{i,z} \\ 0 & N_{i,z} & N_{i,y} \\ N_{i,z} & 0 & N_{i,x} \\ N_{i,y} & N_{i,x} & 0 \end{bmatrix} \tag{3}$$

where $N_{i,x}$, $N_{i,y}$, and $N_{i,z}$ denote the partial derivatives of N_i with respect to x, y, and z. The composite

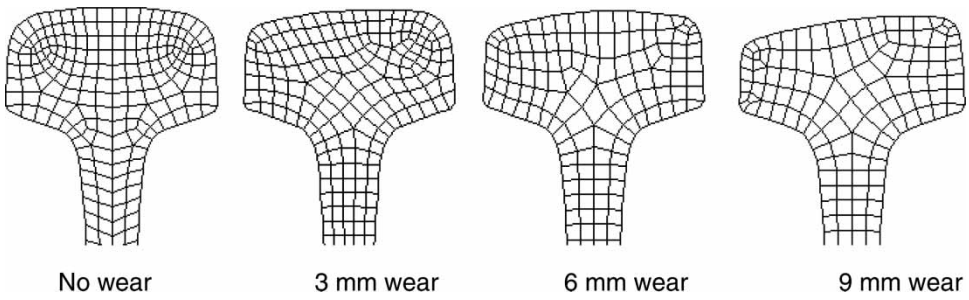

Fig. 3 Wear model of a rail

derivative is

$$\begin{Bmatrix} N_{i,\xi} \\ N_{i,\eta} \\ N_{i,\zeta} \end{Bmatrix} = \begin{bmatrix} x_\xi & y_\xi & z_\xi \\ x_\eta & y_\eta & z_\eta \\ x_\zeta & y_\zeta & z_\zeta \end{bmatrix} \begin{Bmatrix} N_{i,x} \\ N_{i,y} \\ N_{i,z} \end{Bmatrix} = \mathbf{J} \begin{Bmatrix} N_{i,x} \\ N_{i,y} \\ N_{i,z} \end{Bmatrix} \tag{4}$$

where **J** is the Jacobian matrix and

$$x_\xi = \sum_{i=1}^{n} N_{i,\xi} x_i, \quad y_\xi = \sum_{i=1}^{n} N_{i,\xi} y_{,i}, \quad z_\xi = \sum_{i=1}^{n} N_{i,\xi} z_i \tag{5}$$

where n is the number of nodes; then the stress can be calculated

$$\boldsymbol{\sigma} = \mathbf{DB}\boldsymbol{d}^e \tag{6}$$

where **D** is the elasticity matrix. The stiffness matrix of the element can be described according to the above formula

$$\mathbf{K}^{\mathrm{e}} = \int_{-1}^{1}\int_{-1}^{1}\int_{-1}^{1} \mathbf{B}^{\mathrm{T}}\mathbf{DB}|\mathbf{J}|\, d\xi\, d\eta\, d\zeta \tag{7}$$

According to the principle of d'Alembert, the equivalent node force F_I^{e} caused by the element inertia force is

$$\boldsymbol{F}_I^{\mathrm{e}} = -\int_{V^{\mathrm{e}}} \boldsymbol{N}^{\mathrm{T}} \rho_{\mathrm{r}} \ddot{\boldsymbol{u}}\, \mathrm{d}V = -\int_{V^{\mathrm{e}}} \boldsymbol{N}^{\mathrm{T}} \boldsymbol{N} \rho_{\mathrm{r}}\, \mathrm{d}V \ddot{\boldsymbol{d}}^{\mathrm{e}} = -M^{\mathrm{e}} \ddot{\boldsymbol{d}}^{\mathrm{e}} \tag{8}$$

where ρ_{r} is the unit material density of the rail and $\mathbf{M}^{\mathrm{e}}$ is the mass matrix of the element

$$\mathbf{M}^{\mathrm{e}} = \int_{V^{\mathrm{e}}} \boldsymbol{N}^{\mathrm{T}} N \rho_{\mathrm{r}}\, dV \tag{9}$$

2.3 Sleepers

Sleepers can be simplified as Timoshenko beams, whose FEM model is shown in Fig. 4. Each element has two nodes with four degrees of freedom. The equation of every node can be written as

$$\{\delta^{\mathrm{e}}\} = \left[\mu_i^{\mathrm{e}}, \theta_i^{\mathrm{e}}, \left(\frac{\partial \mu}{\partial x}\right)_i^{\mathrm{e}}, \left(\frac{\partial \theta}{\partial x}\right)_i^{\mathrm{e}}, \mu_{i+1}^{\mathrm{e}}, \theta_{i+1}^{\mathrm{e}}, \times \left(\frac{\partial \mu}{\partial x}\right)_{i+1}^{\mathrm{e}}, \left(\frac{\partial \theta}{\partial x}\right)_{i+1}^{\mathrm{e}}\right]^{\mathrm{T}} \tag{10}$$

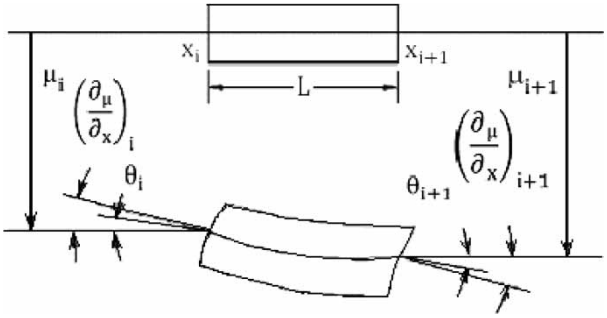

Fig. 4 FEM model of the Timoshenko beam element

where μ is the vertical displacement, θ is the rotation angle caused by bending moment, e is the element number, and i is the node number. Then the displacement function can be described as

$$\mu = \sum_{r=1}^{8} a_r \xi_r^{\mathrm{e}}, \quad \theta = \sum_{r=1}^{8} b_r \xi_r^{\mathrm{e}} \tag{11}$$

where the shape function is

$$\begin{aligned} a_1 = b_2 &= \frac{(2-3\eta+\eta^3)}{4} \\ a_3 = b_4 &= \frac{l(1-\eta)(1-\eta^2)}{8} \\ a_5 = b_6 &= \frac{(2+3\eta-\eta^3)}{4} \\ a_7 = b_8 &= \frac{l(1-\eta)(1-\eta^2)}{8} \\ a_2 = a_4 = a_6 = a_8 &= b_1 = b_3 = b_5 = b_7 = 0 \end{aligned} \tag{12}$$

$\boldsymbol{l}$ is the length of the beam element. The matrices of mass, damping, and stiffness can be derived by the energy method

$$U = \frac{1}{2}EI\int_0^l \left(\frac{\mathrm{d}\theta}{\mathrm{d}x}\right)^2 \mathrm{d}x + \frac{1}{2}\kappa AG\int_0^l \left(\frac{\mathrm{d}\mu}{\mathrm{d}x} - \theta\right)^2 \mathrm{d}x \tag{13}$$

where κ is the shear coefficient, A is the area of the beam unit, E is the elastic modulus, G is the shear modulus, and I is the section modulus.

The unit kinetic energy is

$$T = \frac{1}{2}\rho_s I \int_0^l (\dot{\theta})^2 \, \mathrm{d}x + \frac{1}{2}\rho_s A \int_0^l (\dot{\mu})^2 \, \mathrm{d}x \tag{14}$$

where ρ_s is the unit density of the sleeper and I is the cross-section inertia.

Substituting the displacement function (11) into equations (13) and (14), the expressions for the unit strain energy and kinetic energy may be described as

$$U = \frac{1}{2}\frac{EI}{l}\{\delta^e\}^T[\mathbf{K}]\{\delta^e\}, \quad T = \frac{1}{2}\rho A l^3 \{\dot{\delta}^e\}^T[\mathbf{M}]\{\dot{\delta}^e\} \tag{15}$$

According to the energy method, the derivation of the matrix of stiffness is as follows

$$\begin{aligned} k_{ij} = {} & \frac{2E}{l}\int_{-1}^{1} I \frac{\mathrm{d}b_i}{\mathrm{d}\eta}\frac{\mathrm{d}b_j}{\mathrm{d}\eta}\mathrm{d}\eta + \frac{\kappa G l}{2}\int_{-1}^{1} A\left(\frac{4}{l^2}\frac{\mathrm{d}a_i}{\mathrm{d}\eta}\frac{\mathrm{d}a_j}{\mathrm{d}\eta}\right. \\ & \left. + b_i b_j - \frac{2}{l}b_i\frac{\mathrm{d}a_i}{\mathrm{d}\eta} - \frac{2}{l}b_j\frac{\mathrm{d}a_j}{\mathrm{d}\eta}\right)\mathrm{d}\eta \\ & + \frac{l}{2}\int_{-1}^{1} k_0 a_i a_j \, \mathrm{d}\eta \end{aligned} \tag{16}$$

The derivation of the matrix of mass is as follows

$$\mathbf{m}_{ij} = \frac{\rho l}{2}\int_{-1}^{1} (A a_i a_j + I b_i b_j)\, \mathrm{d}\eta \tag{17}$$

The derivation of the matrix of damping is as follows

$$\mathrm{c}_{ij} = \frac{l}{2}\int_{-1}^{1} c_r a_i a_j \, \mathrm{d}\eta \tag{18}$$

In formulae (16) to (18), k_0 is the supporting stiffness and c_r is the damp coefficient of the sleepers, $i, j = 1, 2, \ldots, 8$.

2.4 The elastic rail pad and fastener model

In this model, the elastic rail pad and the fastener are assumed to be weightless spring elements connecting the bottom of the rail and the rail groove of the sleeper, and the spring and rotational characteristics of the fastener are denoted by rotational and spring stiffnesses, which are shown in Fig. 5.

To connect the rail and the sleeper with the stiffness element, its stiffness matrix is

$$\mathbf{K}^{\mathrm{PE}} = \begin{bmatrix} \mathbf{I}_{\mathrm{RPE}} & -\mathbf{I}_{\mathrm{RPE}} \\ -\mathbf{I}_{\mathrm{RPE}} & \mathbf{I}_{\mathrm{RPE}} \end{bmatrix} \tag{19}$$

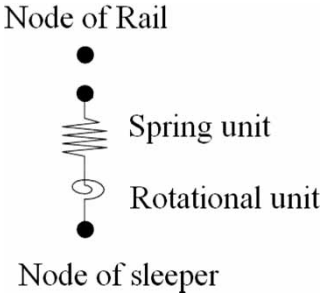

Fig. 5 Model of the rail pad and the fastener

where

$$\mathbf{I}_{\mathrm{RPE}} = \begin{bmatrix} k_1 & 0 & 0 & 0 & 0 & 0 \\ 0 & k_2 & 0 & 0 & 0 & 0 \\ 0 & 0 & k_3 & 0 & 0 & 0 \\ 0 & 0 & 0 & k_4 & 0 & 0 \\ 0 & 0 & 0 & 0 & k_5 & 0 \\ 0 & 0 & 0 & 0 & 0 & k_6 \end{bmatrix} \tag{20}$$

In the above formula, k_1, k_2, and k_3 are the displacement stiffness coefficients of the fasteners, and k_4, k_5, and k_6 are the rotational stiffness coefficients.

From the stiffness, mass, and damping matrices of the rail model, the sleeper model, and the elastic rail pad and fastener model, one can construct the whole stiffness, mass, and damping matrices of the CWR track. Including them into formula (21), one can establish the dynamical balance equation of the CWR system [**16**]

$$[\mathbf{M}]\{\ddot{\boldsymbol{u}}\} + [\mathbf{C}]\{\dot{\boldsymbol{u}}\} + [\mathbf{K}]\{\boldsymbol{u}\} = \{\boldsymbol{F}\} \tag{21}$$

in which [**M**], [**C**], and [**K**] are the matrices of mass, damping, and stiffness, respectively. $\{\boldsymbol{u}\}$ denotes vectors of displacement, and $\{\boldsymbol{F}\}$ is the force.

3 THE FIELD MEASUREMENT

To obtain the data that can be used to check and verify the accuracy of the theoretical computational results, the relationships between longitudinal forces in tracks and vertical vibration characteristics have been measured on the real track. A real normal track under good conditions is chosen for the measurement.

Considering the difficulty in imposing and determining original longitudinal forces on the real track structure, only the rail vertical vibration without the longitudinal force effect on the rail (longitudinal force is equal to zero) is characterized in the beginning. Loosening all the fasteners of the measurement rail can eliminate the longitudinal forces in the rail that will be measured. In a subsequent test, the temperature force is obtained by measuring the change of rail temperature. The parameters of the experiment track are shown in Table 1.

Table 1 Parameters of the experiment track

Rail	60 kg/m (standard of China)
Sleeper	II type (standard of China), 2500 mm long, 250 kg weight
Standard sleeper support spacing	0.6 m
Fastener	I type (standard of China)

The testing procedure is as follows: first, loosen all the fasteners of one rail (25 m long) to ensure that there is no longitudinal force in the rail; second, suspend the sleeper supporting by taking out the elastic pads on the rail ditch of the sleeper, to prevent contact between the rail and the sleeper in the zone of supported spacing according to test requirements; finally, screw the fasteners of the outside unsupported spacing again. The testing state of the rail is shown in Fig. 6. The rail transient vertical vibration response after hammer knock was recorded by a displacement sensor placed at the top of the rail, and the data are shown in Fig. 7. The data of the rail natural vibration was collected and recorded, using a displacement sensor at the top of rail.

Fig. 6 Testing state of the rail

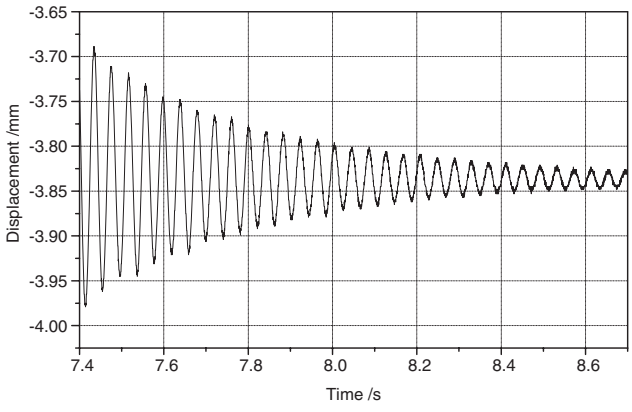

Fig. 7 Time history of the rail's vertical natural vibration response

4 COMPUTATIONAL RESULT AND ANALYSIS OF THE PARAMETERS' INFLUENCE

4.1 Computation parameter

The above-mentioned model is adopted to analyse the vertical vibration characteristics under the longitudinal force of the CWR track. The basic parameters used in the calculation are shown in Table 2.

In the analysis of the track structure, it is necessary to adopt a reasonable modelling length in the dynamic analysis of the CWR track. According to Dong *et al.* [**2**] and Lim *et al.* [**4**], the ideal results can be obtained if the length of the track modelling is more than 200 m long. Table 3 shows the comparison of the first-order rail natural frequencies for the track modelling with different lengths (without longitudinal force). By calculation, it can be found: that the track length (varying from 15 to 200 m) contributes a small variation both to the first-order rail natural frequencies and under the action of longitudinal force.

The calculation results show that the different boundary constraints at both ends of the track have little influence on the results (Table 4). Therefore, it can be considered that relatively accurate results can

Table 2 Basic parameters of the track in the calculation

Rail	60 kg/m (standard of China)
Sleeper	II type (standard of China), 2500 mm long, 250 kg weight
Standard sleeper support spacing	0.6 m
Fastener stiffness	200 MN/m (spring stiffness) 200 kN-m (rotational stiffness)
Foundation stiffness per half sleeper	40 MN/m

Table 3 First-order rail natural frequencies for the track modelling with different lengths (without longitudinal force in the rail)

Length of the modelling	15	25	50	200
First-order rail natural frequency (8.4 m*)	14.510	14.503	14.502	14.502
First-order rail natural frequency (13.2 m*)	6.364	6.171	6.171	6.171

*The length of the sleeper support spacing.

Table 4 Influence of different boundary constraints on both ends of the track (without longitudinal force in the rail)

Boundary constraints	Hinge joint	Fix
First-order rail natural frequency (8.4 m*)	14.510	14.511
First-order rail natural frequency (13.2 m*)	6.364	6.366

*The length of the unsupported sleeper spacing.

be obtained as the natural vibration characteristics of a CWR track are analysed with 25 m modelling length and simple boundary conditions at the two ends of the track (for instance, hinged constraint).

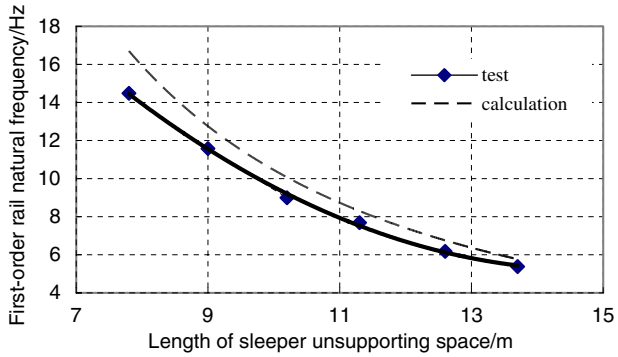

Fig. 8 Comparison of the results of the theoretical calculation and the field measurement

Table 5 Comparison between the calculation of the first-order rail natural frequencies and the results of the field test

Frequency (Hz)	Field measurement result	Calculation result of the finite element model	Theoretical result [2]
Unsupported spacing of sleepers L (m) is 11.3	7.77	8.02	5.15
Unsupported spacing of sleepers L (m) is 13.7	5.4	5.5	3.59

The rail wear is 6 mm and the axial force of the rail is zero.

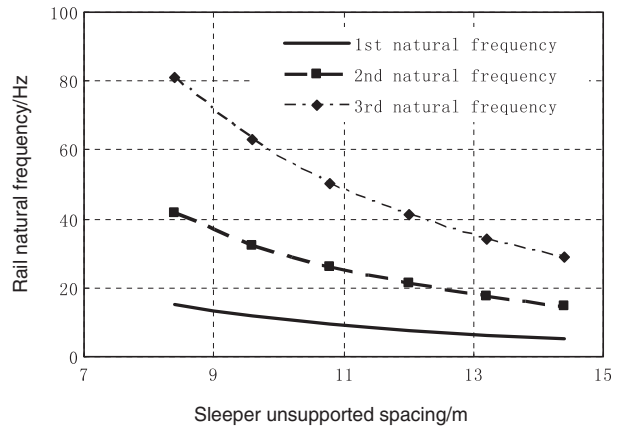

Fig. 9 Rail natural frequencies of the CWR track versus sleeper supported spacing

4.2 Comparison between calculation and measurement

Figure 8 shows the comparison of the results between the theoretical calculation and the field measurement without longitudinal force. As shown in this figure, the longer the unsupported sleeper spacing, the closer the value of two first-order rail natural frequencies. As the unsupported sleeper spacing decreases, the difference between the measured and computed results increases.

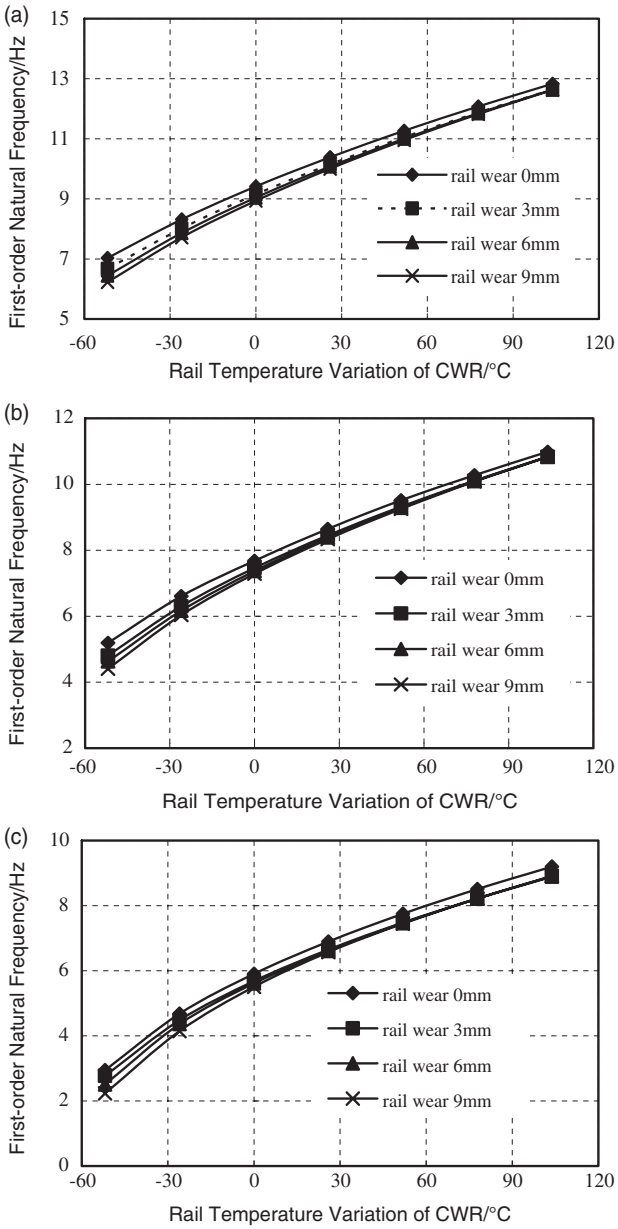

Fig. 10 First-order rail natural frequencies versus rail temperature force variation of the CWR at different wear levels of the rail: (a) unsupported sleeper spacing of 10.8 m, (b) unsupported sleeper spacing of 12 m, and (c) unsupported sleeper spacing of 13.8 m

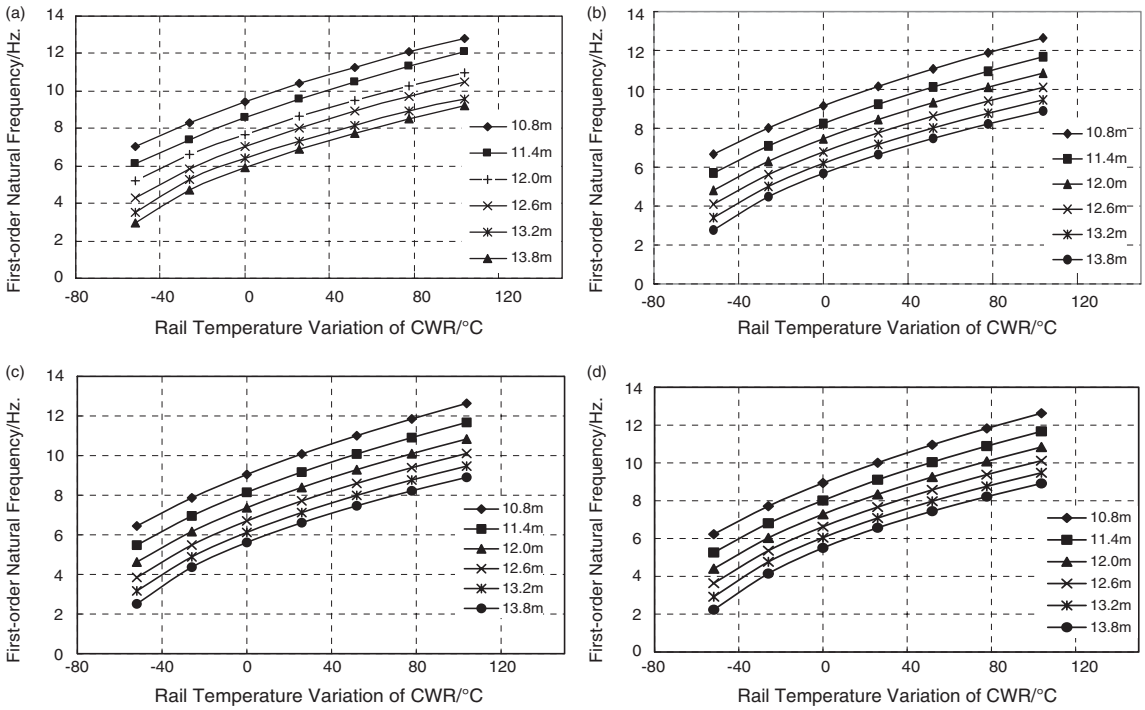

Fig. 11 First-order rail natural frequencies versus rail temperature variation of the CWR at different unsupported sleeper spacings: (a) rail wear of 0 mm, (b) rail wear of 3 mm, (c) rail wear of 6 mm, and (d) rail wear of 9 mm

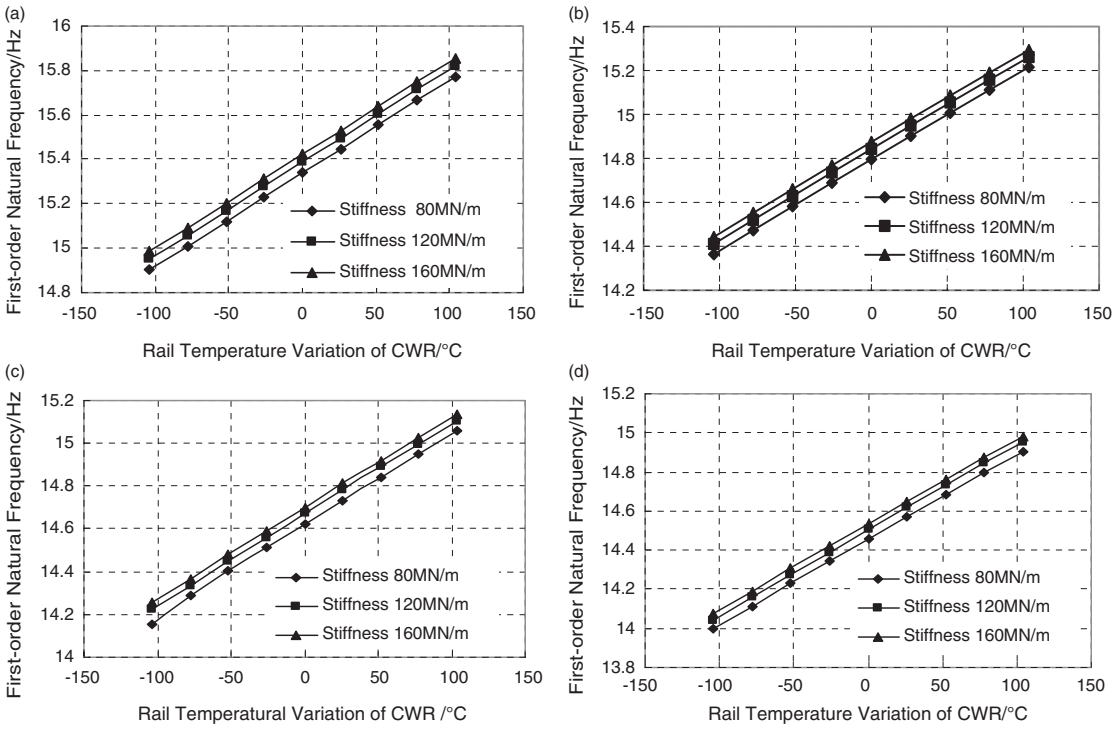

Fig. 12 First-order rail natural frequencies versus rail temperature variation of the CWR at different foundation stiffness: (a) rail wear of 0 mm, (b) rail wear of 3 mm, (c) rail wear of 6 mm, and (d) rail wear of 9 mm

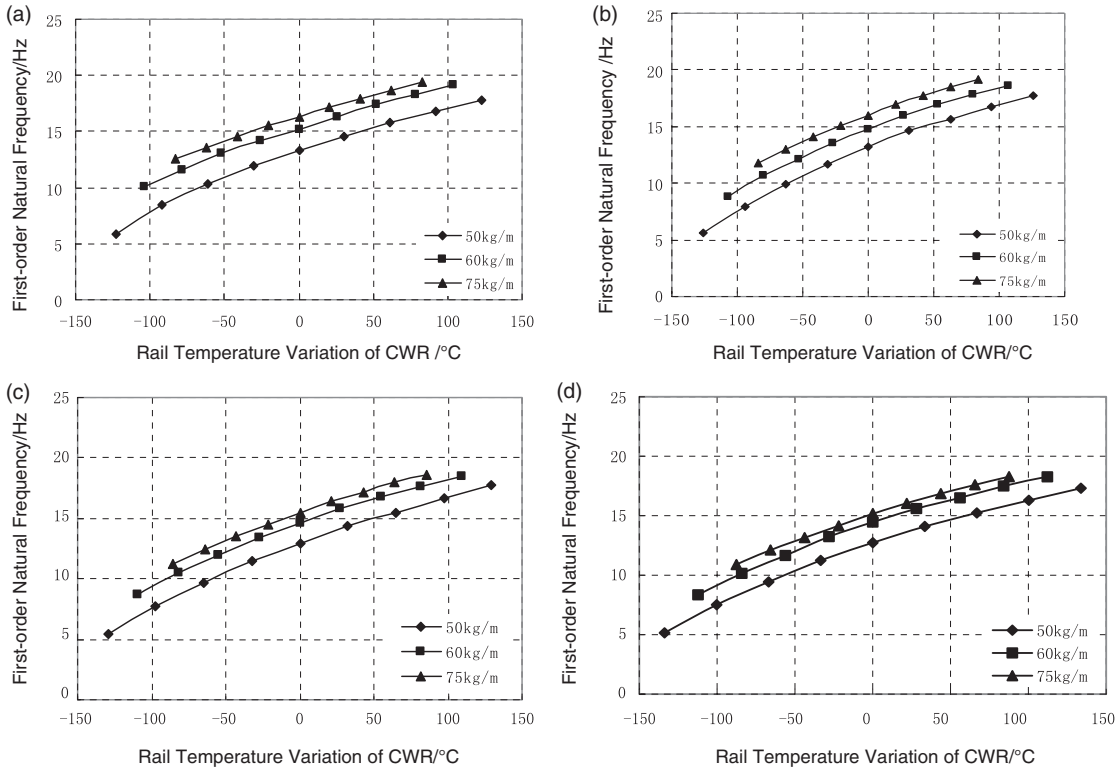

Fig. 13 First-order rail natural frequencies versus rail temperature variation of the CWR at different types of rails: (a) rail wear of 0 mm, (b) rail wear of 3 mm, (c) rail wear of 6 mm, and (d) rail wear of 9 mm

The comparison of the results of the theoretical calculation and the field measurement is shown in Table 5.

The comparison shows that there is good agreement between the calculation results of the finite-element model and the field measurement results. The relative error is larger when the simplified rail model [**11**] is applied.

4.3 Analysis of parameters effect

Figure 9 shows the influence of the sleeper support spacing on the rail natural frequencies. The rail natural frequency drops when the unsupported sleeper spacing increases, but the descendent tendency seems to become smooth while the unsupported sleeper spacing increases. The variation range of the first-order natural frequencies is relatively less than that of the second-order natural frequencies. The higher the order, the larger the variation range.

4.3.1 Effect of rail wear

It can be seen from Fig. 10 that the rail wear has some effect on the rail natural frequencies of the CWR track. The rail natural frequencies decrease with an increase in the rail wear. This change is more obvious when the rail is under compressive stress.

4.3.2 Effect of sleeper spacing

Figure 11 shows the relationship between the first-order rail natural frequencies and the rail temperature (the longitudinal force of the rail) variation when the unsupported sleeper spacing is changed with different states of the rail wear. The relationship between temperature change of the rail and the longitudinal force is

$$P_t = E\alpha\Delta TA \tag{22}$$

where different variables and parameters are defined as follows: P_t is the longitudinal force of the rail, E is Young's modulus for the rail, A is the total cross-sectional area of the rail, α is the linear expansion coefficient of the rail steel, and ΔT is the temperature change of the rail (defined as $\Delta T = T_{\text{actual}} - T_{\text{initial}}$).

It may be concluded from Fig. 11 that the rail natural frequencies decrease with a decrease in the longitudinal force due to rail temperature variation. Also, the wear of the rail will have an effect on the relationship between the rail natural frequencies and the longitudinal force.

4.3.3 Effect of foundation stiffness

The foundation stiffness of the CWR track has a certain effect on the relationship between the first-order

rail natural frequencies and the rail temperature (longitudinal force of the rail). The figures vary when the foundation stiffness is changed with different states of the rail wear, as shown in Fig. 12. It can be seen from Fig. 12 that the rail natural frequency decreases with a decrease in the foundation stiffness of the CWR track. It can also be seen from the figures that the wear of the rail will have no significant effect on the relationship between the rail natural frequencies and the foundation stiffness.

It has been found that the influences of the stiffness of rail pads and fastener, including the elastic and rotational stiffnesses, on the rail natural frequencies of the CWR track are weak. Hence these parameters can be ignored in the analysis of the dynamic characteristics of the rail under the temperature force in the CWR track.

4.3.4 Effect of rail types

The influences of different rail types on the relationship between the first-order rail natural frequencies and the rail temperature variation are shown in Fig. 13. The type of rail has a significant effect on the first-order rail natural frequencies because both the mass and cross-section have changed in different types of rails. The heavier the rail, the more important the effect on rail natural frequency.

5 CONCLUSIONS

This article presents a dynamic model that indicates the inherent relationship between the vibration characteristics of the CWR track structure and the rail temperature force. The finite-element model is set up by considering the rail section profile and the elastic and rotational stiffnesses of the fasteners. The model takes into account the influence of parameters such as the rail type, the state of the rail wear, the spring stiffness and rotational resistance stiffness in the rail pad and fastener elements, the sleeper support spacing, and the foundation stiffness. The correlation between the vibration characteristics of the rail and the change of the longitudinal force (rail temperature) has been established by using this model, and the effects of various track parameters have also been investigated.

Computational results in the finite-element model are in good agreement with those obtained from the simplified model [**11**]. This shows that the longitudinal force has a great influence on the rail natural frequencies. The lower-order rail natural frequencies will increase when the longitudinal force increases, and vice versa. High-order natural frequencies are largely affected by the change of the longitudinal force. The results agree well with those of the field measurement, compared to the simplified beam formulation in reference [**11**].

It is concluded from the study that increasing the unsupported sleeper distance may decrease the rail natural frequencies, and the high-order frequencies are affected more. When different types of rails are used in the CWR track, the influences caused by the longitudinal force on the rail natural frequencies will also be affected. The heavy-type rail tracks can reduce the dependency of natural frequencies on the longitudinal force to some extent. The wear of the rail, which will increase the influences on the rail natural frequencies, also has an influence on the correlation between the longitudinal force and the rail natural frequencies. The elasticity of the ballast has relatively less influence on the natural frequency than other parameters. The influence mentioned above will increase when the elasticity decreases. The rail pad and fastener stiffnesses, including the elastic stiffness and the rotational resistance stiffness, have weak influences. Finally, the following remarks can be made from the present study.

1. Under different longitudinal forces, the vibration response character of the CWR track structure will have corresponding changes. The increase in longitudinal force may lead to a decrease in rail natural frequencies and vice versa. The higher the vibration frequency, the greater the influence. This correlation is very important to understand the dynamic characteristics of the rail under the temperature force and explore non-destructive measurement of the temperature force of the real CWR track.
2. The unsupported sleeper spacing has a significant influence on the rail natural frequencies and note that the higher the vibration frequency, the greater the influence. The influence of this factor should be considered in the vibration analysis of the CWR track.
3. Different types of rails of CWR tracks may affect not only the rail natural frequencies, but also the track stability under the temperature force. The wear of the rail in the track will have a certain effect. As a result, the factor mentioned above should be considered in track maintenance.
4. Although the foundation stiffness has some effects on the dynamic characteristics of the CWR track, the influences are weak. The ballast will have a low stiffness after being maintained and renewed. The foundation stiffness of the track increases gradually with operation.
5. Because of their weak influence on the vibration characteristics, the rail pad and fastener stiffnesses, including the elastic stiffness and vertical rotational resistance stiffness, can generally be ignored in the analysis of the CWR track.

ACKNOWLEDGEMENTS

The work reported here was funded by the National Natural Science Foundation of China (grant number 50378070). The authors are grateful for this support. They express their thanks to the master candidates: Tan Dazheng, Wang Xianghao, Fu Yifan, and Liu Yan for their help during the field measurement.

REFERENCES

1 **Esveld, C.** *Modern railwaytrack*, 2001 (MRT-Productions, Zaltbommel).
2 **Dong, R. G., Sankar, S.,** and **Dukkipati, R. V.** A finite element model of railway track and its application to the wheel flat problem. *Proc. IMechE, Part F: J. Rail and Rapid Transit*, 1994, **208**(F1), 61–72. DOI: 10.1243/PIME_PROC_1994_208_234_02.
3 **Yanag, H.** and **Kataoka, H.** Analytic research on the compressive yield safety of long rail. *Railw. Res. Rev.*, 2001, **57**(1), 18–21.
4 **Lim, N.-H., Park, N.-H.,** and **Kang, Y.-J.** Stability of continuous welded rail track. *Comput. Struct.*, 2003, **81**, 2219–2236.
5 **Lei, X.** and **Feng, Q**. Analysis of stability of continuously welded rail track with finite elements. *Proc. IMechE, Part F: J. Rail and Rapid Transit*, 2004, **218**(F3), 225–234. DOI: 10.1243/0954409042389409.
6 **Miurn, S.** Lateral track stability: theory and practice in Japan. In Lateral Track Stability 1991: Proceedings of a Conference, St. Louis, Missouri, 1991, pp. 53–63 (Transportation Research Board, Washington, DC).
7 **Lou, P., Cheng, X.,** and **Zeng, Q.** Probabilistic analysis of lateral initial irregularities of continuously welded rail track. *J. Struct. Eng.*, 2002, **29**(2), 175–176.
8 **Bao, Y.** and **Barenberg, E. J.** Three dimension nonlinear stability analysis of tangent CWR track under temperature and mechanical loads. *Transp. Res. Rec.*, 1997, **1584**, 31–40.
9 **Kish, A.** and **Samavedam, G.** Dynamic buckling of continuous welded rail track: theory, test, and safety concepts. In Lateral Track Stability 1991: Proceedings of a Conference, St. Louis, Missouri, 1991, pp. 23–38 (Transportation Research Board, Washington, DC).
10 **Kish, A.** Analysis of phase 3 dynamic buckling test, Report no. DOT-TSC-FRA-89-2, Transportation System Center, 55 Broadway, Kendall Square, Cambridge, MA 02142, USA, 1990.
11 **Luo, Y.** A model for predicting the effect of temperature force of continuous welded rail track. *Proc. IMechE, Part F: J. Rail and Rapid Transit*, 1999, **213**(F2), 117–124. DOI: 10.1243/0954409991531074.
12 **Samavedam, G., Kish, A., Purple, A.,** and **Schengart, J.** Parametric analysis and safety concepts of CWR track buckling, Report no. DOT-ORD-93-26, National Technical Information Service, Washington, DC, 1993.
13 **Hou, K., Kalousek, J.,** and **Dong, R.** A dynamic model for an asymmetrical vehicle/track system. *J. Sound Vibr.*, 2003, **267**, 591–604.
14 **Gustavson, R.** and **Gylltoft, K.** Influence of cracked sleepers on the global track response: coupling of a linear track model and non-linear finite element analyses. *Proc. IMechE, Part F: J. Rail and Rapid Transit*, 2000, **216**(F1), 41–51. DOI: 10.1243/0954409021531674.
15 **Grassie, S. L., Gregory, R. W., Harrison, D.,** and **Johnson, K. L.** The dynamic response of railway track to high frequency vertical excitation. *Proc. Instn Mech. Engrs: J. Mechanical Engineering Science*, 1982, **24**, 91–95.
16 **Clough, R. W.** and **Penzien, J.** *Dynamics of structures*, 1975 (McGraw-Hill, New York).

APPENDIX

Notation

a_r	shape function of vertical displacement
A	area of the beam element
b_r	shape function of the rotation angle
c_{ij}	element in the matrix of damping, $i, j = 1, 2, \ldots, 8$
c_r	damp coefficient of the sleepers
$[\mathbf{C}]$	matrices of damping
$\boldsymbol{d}$	displacement vector of a node in the system
$\mathbf{D}$	elasticity matrix
e	number of elements
E	elastic modulus
$\{\boldsymbol{F}\}$	force
F_I^{e}	equivalent node force
G	shear modulus
i	node number
I	cross-section inertia
I	section modulus
$\mathbf{J}$	Jacobian matrix
k_i	displacement stiffness coefficient of the fasteners, $i = 1, 2, 3$
k_{ij}	element in the matrix of stiffness
k_j	rotational stiffness coefficient of the fasteners, $j = 4, 5, 6$
$\mathbf{K}^{\mathrm{e}}$	stiffness matrix of the element
$\mathbf{K}^{\mathrm{PE}}$	stiffness matrix including the rail and the sleeper
$[\mathbf{K}]$	matrices of stiffness
$\boldsymbol{l}$	length of the beam element
$\boldsymbol{L}$	differential coefficient operator
$\mathbf{m}_{ij}$	element in the matrix of mass
$[\mathbf{M}]$	matrices of mass
$\mathbf{M}^{\mathrm{e}}$	mass matrix of the element
n	number of nodes
N_i	shape function of node i
$N_{i,x}$	partial derivative of N_i with respect to x
$N_{i,y}$	partial derivative of N_i with respect to y
$N_{i,z}$	partial derivative of N_i with respect to z
P_{t}	longitudinal force of the rail
T	unit kinetic energy
ΔT	temperature change of the rail (defined as $\Delta T = T_{\mathrm{actual}} - T_{\mathrm{initial}}$)

$\boldsymbol{u}$	random displacement vector of an element
U	unit strain energy
α	linear expansion coefficient of the rail steel
ε	element strain
ζ_i	natural coordinates of node i in the z-direction
η_i	natural coordinates of node i in the y-direction
θ	rotation angle caused by the bending moment
κ	shear coefficient
μ	vertical displacement
ξ_i	natural coordinates of node i in the x-direction
ρ_{r}	unit material density of the rail
ρ_{s}	unit density of the sleeper
$\boldsymbol{\sigma}$	stress